Research Square

Preprints are preliminary reports that have not undergone peer review.
They should not be considered conclusive, used to inform clinical practice,
or referenced by the media as validated information.

Design of An Energy Efficient Toggled MRAM Bit-Cell

Divyansh Jain
Lovely Professional University
Haziqul Yaquin
hyaquin@gmail.com

SND College of Engineering and Research Center

Research Article

Keywords: Non-volatile memory, Toggle spin torque, VCMA effect, magnetic random-access memory, micromagnetics, magnetic interface

Posted Date: August 3rd, 2026

DOI: https://doi.org/10.21203/rs.3.rs-10477068/v1

License: This work is licensed under a Creative Commons Attribution 4.0 International License.
Read Full License

Additional Declarations: No competing interests reported.

Design of An Energy Efficient Toggled MRAM Bit-Cell

Divyansh Jain[1] & Dr. Haziqul Yaquin[2]*

[1]Research and Development Cell, Lovely Professional University, Phagwara, Punjab-144411, India, divyanshdinesh1996@gmail.com

[2]Department of Electrical Engineering, SND College of Engineering and Research Center, Nashik, Maharashtra-423401, India, *hyaquin@gmail.com

ABSTRACT

Spin-based, non-volatile memory bit-cells have been proposed for applications ranging from logic-in-memory computing to quantum computing. This paper deals with the toggle spin torque magnetic random-access memory (TST-MRAM) bit-cells by micromagnetic simulations. The concept of voltage-controlled magnetic anisotropy (VCMA) is utilized to model and simulate the designed cells. In this paper, the TST magnetization precession is studied in a nanopillar spin-valve. The magnetization switching is considered under an external magnetic field, and it is simulated with the micromagnetic simulation (MMS) toolkit to evaluate the designed toggled MRAM bit-cell parameters. The present work utilizes different material interfaces (i.e., HM-CoFeB-NM-MgO) to minimize the switching error rates during the MRAM design process. The interfacial perpendicular magnetic anisotropy-based toggled MRAM bit-cell obtains less polarization factor, more anisotropic constant, and less saturated magnetization than classical magnetic RAM models. The factors related to the designed bit cell are explained theoretically and graphically in this work. Finally, the parameters have been evaluated for the proposed toggled MRAM bit-cell and will take part in the design process.

Keywords: *Non-volatile memory, Toggle spin torque, VCMA effect, magnetic random-access memory, micromagnetics, magnetic interface.*

1. INTRODUCTION

Next-generation nanoelectronic devices consume very little power while increasing memory storage and processing capabilities [1-2]. These devices use the degree of freedom associated with the spin of electrons [3] combined with their orbital moments. Magnetoresistive random-access memory (MRAM) encodes information through magnetic domain alignment, holds the promise to surpass rival technologies, and emerges as a ubiquitous memory solution. MRAM has evolved to utilize the benefits of traditional memory technologies, i.e., SRAM, DRAM, and flash memory [4-6], and plays a crucial role in semiconductor markets. MRAM information is stored in magnetic moments [7], but electric charge or current flows across the junction are not stored. Much effort has led to the commercialization of spin-transfer torque magnetic random-access memory (STT-MRAM) [8-13] due to their nonvolatility [14-17], unlimited endurance [18], low power consumption, better CMOS adaptability, lower read-write access time, and high-speed operation [19-23]. The main building block of the STT-MRAM cell is a magnetic tunnel junction (MTJ), which comprises two magnetic layers separated by a thin insulating layer. A storage device is made from a large-scale grid [24] of such single-bit memory cells. Conventional MTJs contain in-plane magnetic anisotropy (IMA) for the magnetic layers [25-27]. Due to the symmetry breaking at the interfaces, the coupling effect occurs, and it is termed interfacial perpendicular magnetic anisotropy (iPMA). This anisotropy doesn't depend on the intrinsic characteristics of thin Fe films. The spin Hall effect (SHE) and magnetic anisotropy effect are proposed for enhancing the performance of STT-MRAM [3]. Due to the finite TMR ratio, a high write current (~100 μA) and the lower sense edge [4-5] are the two most significant concerns for the commercialization of STT-MRAM. The drawback of high write current lies in the increased demand for data manipulation [6], thereby constraining the transistor's scalability [7]. Due to the poor spin-infusion efficiency and the least-resistance write method, SHE model-based memory bit-cells are widely used. Voltage-controlled magnetic anisotropy (VCMA) has mainly been intended for novel TST-MRAM cell development [26].

A branch of spintronics or magnetism termed as magnonics. Related to its predecessors, phononics and photonics, it relies on the fundamental resonance of magnetic structures known as spin waves or magnons in the subatomic limit, which are capable of carrying energy and information. In addition to providing information, spin waves can convey energy and both linear and angular motion. Because of their exceptionally low damping and lack of Joule heating, magnetic insulators [28], i.e., YIG ($Y_3Fe_5O_{17}$) are the best possible materials for manipulating spin waves. Additionally, spin waves are capable of interacting with magnetic

textures [29], such as magnetic domain barriers and skyrmions, introducing a novel method of accessing magnetic memories. Furthermore, the advancement of research in spin physics relies on the supervision of antiferromagnetic electric fields. The antiferromagnetic (AFM) material [30] is more immune to magnetic field disturbances. The MRAM's micromagnetic effect demonstrates the magnetization behavior on a deep sub-micron scale. The micromagnetic theory, which involves classical field theory with quantum mechanical effects, is semiclassical. The micromagnetic theories consolidate quantum mechanical effects in ferromagnets, including exchange interaction and magnetization dynamics. In contrast to the macroscopic Maxwell equations, the micromagnetic model considers the magnetic domains and domain wall structures. This process empowers exact hysteresis calculations of macroscopic magnets resulting from field-induced domain generation origination and annihilation. Aside from the magnetization with external fields [31], the synergy of spin-polarized currents with the magnetization shows a flourishing role for unique devices. In this paper, the authors have proposed a TST-MRAM cell design using the voltage-controlled magnetic anisotropy (VCMA) effect with the help of a micromagnetic simulator (NIST-Simulmag). The novelty features of the present work are represented as:

1) The proposed VCMA-based toggled MRAM bit-cell facilitates fast switching and extremely low switching power thanks to its low damping ratio, high anisotropy coefficient, and large magnetic polar orientation in the z-direction.
2) In order to enhance the stability of the proposed toggled MRAM bit-cell, it is necessary to consider the azimuthal orientation in a focal plane, a factor typically overlooked in classical magnetic memory design.
3) The micromagnetic effects are taken into account in the design, which provides deep insight into the parameters like magnetization factor, and polar and azimuthal orientation required for novel toggled MRAM bit-cell design.

C. Abert *et al.*, used the spin transport phenomena across tunnel barriers, which are controlled by quantum mechanical material, and produced a computational model based on micromagnetism and spin physics. They have employed the denoising technique, which made a big impact on spintronics memories while also being highly accurate and consuming relatively lower computing time [32]. D. Jain *et al.*, proposed a circuit modeled TST-MRAM bit-cell by employing VCMA and Rashba spin-orbit interaction (SOI) effect [33]. The read-write access time, magnetization, and switching speed have been improved by the proposed circuit model. R. Hao *et al.*, proposed a novel SAF-FL-MRAM through MMS. They demonstrated the reduction in switching current by 20 times utilizing the RKKY interaction in the SAF-FL of

MTJ. The attained switching current for writing speed was sufficient for the restoration of SRAM in the L2 cache, as noted in reference [34]. SRAM restoration. C. Yoshida *et al.*, presented the fast-probabilistic switching action in the double MgO MTJ with low impacted and pillar formation. They realized the back-hopping anomaly for A.P. to P switching for the MTJ pillar framework but found no back-hopping abnormality with the stepped framework. They validated that this back-hopping was guided by combining the stray field from the pinned layer and the VCMA effect [35]. STT magnetization precession in Co/Cu/Co nanopillars has been predicted micro magnetically by H. B. Huang *et al.* It is subdivided into four types: unchanging state (U.N.), precessional state (P.S.), multidomain state (M.S.), and bistable state. (B.S.). P.S. can further be divided into two types based on four states: steady precession and sub-steady precession modes [36]. P.F. Carcia *et al.*, observed the structural and magnetic properties of a Pd/Co thin film and calculated the magnetic anisotropy in this structure. They have also found the anisotropy field and total anisotropic energy with Co layer thickness [37] and it is used in spintronics memory development. To carry out a computing process in the bit-cell array, J. Wang *et al.* introduced a programmable bit serial operation. Bit-serial computing in memory (BSCIM) architectural optimization [38] has been carried out using the toggle spin-orbit torque magnetic random-access memory (TSOT-MRAM) cell. They indicate the reduction in delay time, improvement in throughput, and increase in energy efficiency. Now with the aid of spintronics, Y. Zhang *et al.*, proposed a time domain computing in memory (TD-CIM) approach that can be employed to build an energy-efficient conventional neural network (CNN) using spintronics. They utilize digit recognition on the MNIST dataset [39] to demonstrate the improvement in energy needs and duty cycle.

The rest of this paper is classified as follows. Section 2 describes the detailed TST-MRAM bit cell design with the various interface-associated structures formulated by mathematical equations. It also accords with the physics involved in the designed toggle-based MRAM cell and its switching mechanism. Section 3 shows the micromagnetic simulation results using the VCMA effect for designing the TST-MRAM bit cell to provide an alternative non-volatile memory technique. Thus, the manuscript has been concluded in Section 4.

2. PROPOSED MRAM DESIGN

2.1. Magnetic layered interfaces for Toggled MRAM

The spin interface within TST-MRAM denotes the point of connection between a ferromagnetic layer and a nonmagnetic layer, both influenced by the presence of a heavy metal (H.M.) layer. The interaction of spin and orbital properties allows for the manipulation of the hybridization between the ferromagnetic and nonmagnetic materials. These interfaces

consist of 2D layers situated between the ferromagnetic free and fixed layers. The spin-valve effect alters the composition and properties of these interfaces and can be used for hybrid MTJs. Different material interfaces like F.M.-N.M. layer interface, F.M.-H.M.-N.M. layer interface, and NM-FM interfaces are employed for designing the MRAM cells (for example, Ru, Ta, Mo, etc.). The following part discusses the design specifics and modeling of the TST-MRAM cell that exploits interface properties to generate the spin-valve effect. In addition, we discuss heavy metal miniaturization in MRAM cells.

2.2. H.M./F.M. interfacial modulation for strong PMA

STT-MRAM has some demerits, such as low adaptability and the lowest STT switching efficiency. In this paragraph, we discuss perpendicular magnetized MTJs (p-MTJ) for applications in planar chips. The magnetization switching H.M./F.M. multilayer is induced by spin-orbit torque (SOT). This multilayer follows the Dzyaloshinskii-Moriya interaction (DMI) between molecules. The chiral domain nucleation supervises this process at the interfaces. The HM/FM interface stiffness plays a vital role in the DMI process. It directly reflected the outcomes of this process in the spin-orbit torque of the MRAM cell. Hence, the surface of the HM/FM multilayer becomes smooth due to the absence of impurities [41-42]. The CoFeB film's magnetic property and thermal stability have altered the H.M./F.M. interfacial modulation. The PMA can be induced by thin film epitaxial growth with the effect of bond orientation and interfacial interface in the buffer layer.

2.3. PMA in cobalt-dependent multilayers

Interfacial perpendicular magnetic anisotropy (iPMA) occurs at Co/Pt interfaces or junctions in MTJ due to the Co layer's presence. The combination of noble metal Pt and Co generates interfacial perpendicular magnetic anisotropy (iPMA) with the <111> texture [40-41]. The Co/Pt multilayer consists of a free layer and a reference layer in the p-MTJ structure. Due to the lower spin polarization coefficient, the TMR ratio is lower in Co/Pt multilayers [42-43]. However, Co/Pt multilayers require a high threshold current for magnetization switching and are employed as a bottom reference layer in p-MTJ with the help of iPMA, as shown in Fig. 1. Unlike the Co-Fe/Pd multilayers [44], achieving equilibrium in the three-state system through spacer layers doesn't necessitates the separate arrangement for GMR signal evaluation. The TMR ratio of a thermally robust p-MTJ is 1.5 when the annealing process [45] is applied at the interface for 30 minutes. The isothermal annealing has been used in this process with a critical temperature of 400^0C. It can be employed to enhance the workability and toughness of the material. It is a less costly and faster process as compared to complete annealing of the specified material.

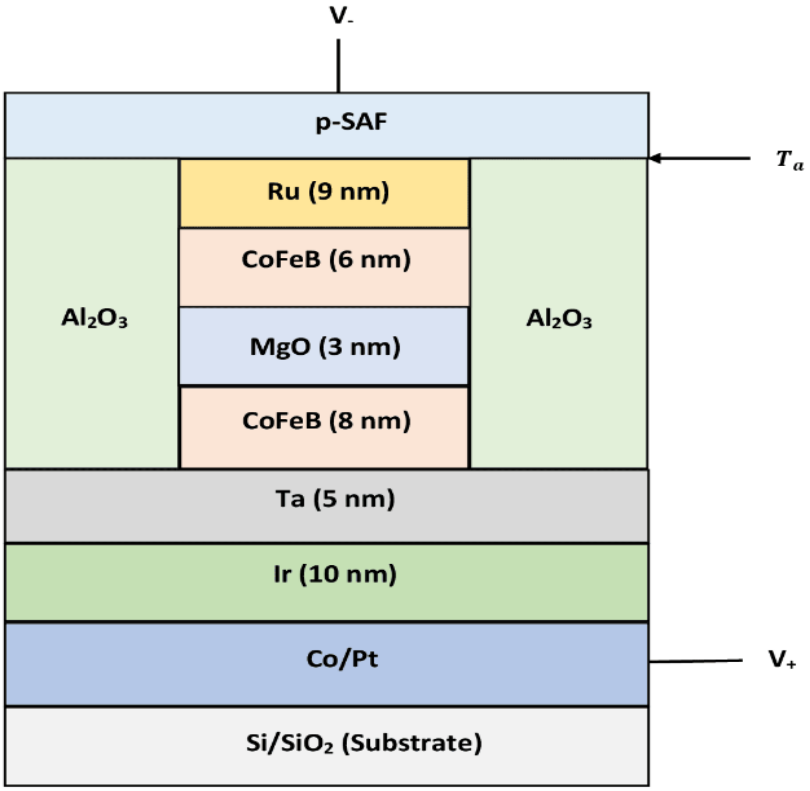


Figure 1: *Schematic of the iPMTJ structure for CoFeB/MgO domains with Co/Pt multilayers. Schematic concept adapted from [26].*

The p-type synthetic antiferromagnetic (p-SAF) coupled reference structure is used at the spin transistor. The spin transistor is developed by a magnetic semiconductor and is a magnetically sensitive device. Yakushiji [46] stated that the p-SAF system with inter-layer exchange coupling (IEC) and Ru layer could replace the Co/Pt multilayer structure. This p-SAF reference layer is embedded in the p-MTJ form and shows a TMR ratio of 1.45. The bottom Ru layer is replaced with an Ir layer when the IEC energy density variation occurs.

The MTJ conductance can be represented as a 2x2 matrix whose diagonal elements can be expressed as:

$$G_{11} = G_{22} = G_0(1 + P_1P_2.cos\,\theta)\,, \qquad (1)$$

G_{11} and G_{22} represent the MTJ conductance matrix's diagonal elements, while G_0 is the average of the MTJ conductance of parallel and antiparallel configurations. P_1, P_2, and θ represent the spin polarization coefficients of MTJ and a spin polarization angle, respectively. The non-diagonal elements of the MTJ conductance matrix are related to the diagonal elements, expressed as:

$$G_{12} = -G_{11}\,, \quad G_{21} = -G_{22}\,. \qquad (2)$$

The Co/Ni multilayers give rise to a tunable iPMA with large spin polarization [47] and a lower damping ratio [48] for the free layer. Such multilayers are bounded by the considerable

magnetic anisotropic energy (MAE) at the location of iPMA. The spin current is generated from the interface between thin Co and Ni layers. The iPMA occurs at a magnetic interface with spin-orbit coupling (SOC) [49] and gives rise to magnetoelastic anisotropy [50] for the free layer. Due to the strong magnetic anisotropy, these multilayers are used as reference layers in p-MTJs. The TMR ratio of 1.45 or 145% is obtained in a Co/Ni-based p-MTJ stack with a channel thickness of 10.6 nm [51].

2.4. PMA in F.M./CoFeB/MgO structures

The FM/CoFeB/MgO interface-based MTJ [52-53] gives rise to a TMR ratio of 124%, a thermal stability of 43, and a switching current of 49 μA at the magnetic interface. The channel length of the CoFeB composite is $20nm$. The thermal stability coefficient Δ [54] is represented as:

$$\Delta = \frac{E_B}{k_B T} = \frac{KV}{k_B T}, \quad (3)$$

Here E_B is the energy barrier between the parallel and antiparallel states for the magnetization in the free and reference layers. $k_B, T, K,$ and V represent Boltzmann's constant, room temperature, anisotropy energy density, and the free layer's volume. For example, the anisotropy energy density of the free layer of the CoFeB composite [55] is represented as follows:

$$K = M_s\left(\frac{|\vec{H}_a|}{2}\right) = \frac{K_i}{t_{CoFeB}} + K_b - 2\pi M_s^2, \quad (4)$$

where $K_i, M_s, |\vec{H}_a|$ are the interfacial magnetic anisotropy, saturation magnetization, and magnitude of the anisotropic field. K_b is the bulk magnetic anisotropy and t_{CoFeB} is the thickness of the CoFeB-free layer. The Ta/CoFeB/MgO structure demonstrates in-plane magnetic anisotropy when the CoFeB layer is very thin. The enhancement of magnetic anisotropy is not possible when the CoFeB layer thickness is $1.3nm$.

The prevalent assumption is that the 2p orbitals of oxygen atoms in tandem with spin-orbit coupling represent the place where surface iPMA originated from. The process of over-oxidation or under-oxidation at the interface reduces the effective hybridization between the $3d$ orbitals of Fe and the 2p orbitals of O atoms. Spin-orbit coupling (SOC) causes a rapid decrease of iPMA at the interface. The aspect ratio is defined as the ratio of the width and height of the magnetic layer, and this ratio of the Fe/MgO structure [56] is determined for the free layer. It is found that the PMA occurs at the interfacial Fe monolayer in the CoFeB composite and transports interfacial magnetic anisotropy into the Fe/Ru monolayer. These interfacial conditions result in the occurrence of iPMA at the Fe/MgO interface [57]. The p-

MTJ with Ta/CoFeB/MgO structure is represented in Fig. 2. This MTJ is formed in conjunction with the ferromagnetic layer CoFeB and nonmagnetic layer MgO, along with Al_2O_3 spacer layers. The bulk material is SiO_2 with the Ta and Ru material layer interfaces and the FM-NM layer interface. This structure forms the Stoner particle domain and follows the Stoner principle.

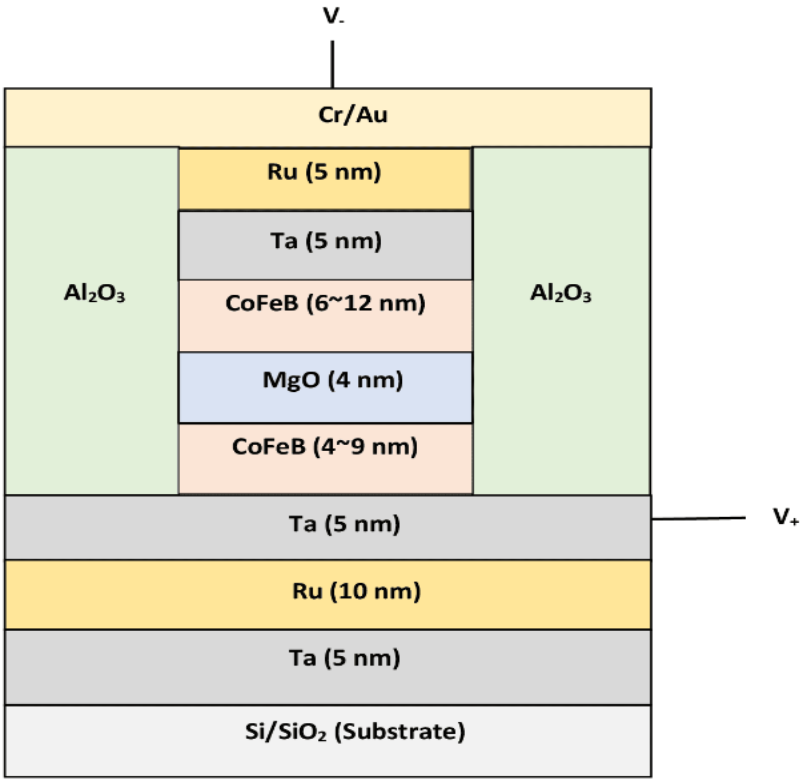


Figure 2: *Schematic of the MTJ structure for in-plane and out-of-plane magnetization for CoFeB/MgO domains.*

2.5. PMA in H.M./CoFeB/MgO structures

Strong PMA and considerable thermal stability are required to store the information in MTJ. When the storage limit of memory increases, the strong PMA ensures a lower chip deterioration rate and higher data retentivity. A thermal stability factor of 75 is required for a 128 GB memory chip. This factor is essential to accomplishing a data confinement time of at least 10 years and a chip deterioration rate [58-61] of 10^{-4} in particular MTJ. A higher anisotropic field is required to get an optimized MRAM performance. The interfacial PMA occurs at a Ta/CoFeB/MgO interface [62], and a free layer surface PMA must be lower than 4.7 mJm^{-2}. Generally, the applied flux density is less than 2 mJm^{-2}, but the required flux density of the iPMA system is greater than 3.1 mJm^{-2}. Due to the required flux density, the data confinement time is less than $1ms$ for cache memory. Hence, it is essential to improve PMA for the large density of MRAM cells.

Some researchers have investigated the impact of annealing temperature on magnetic anisotropy, and PMA is increased at an annealing temperature of 350°C [53], [63]. When the annealing temperature is less than 350°C, the Ta/CoFeB/MgO composite does not develop the required strength of PMA-implanting the Ta layer along with the z-axis results in thermal saturation of magnetic flux at 400°C, which interferes with the coordination with CMOS circuits. Fig. 3 represents the p-MTJ stack with the H.M./CoFeB/MgO composite. The ferromagnetic composite (CoFeB) channels are $1.3nm, 1nm$, and $0.5nm$ long with a nonmagnetic composite layer (MgO), which provides the interlayer interfacing. The interlayer (FM-HM-MgO) interface contains a W spacer of $0.2nm$ and a W bridge of $0.3nm$ with Ta metal for a higher saturation magnetization and lower read and writes access time in the MRAM cell. The free layer of MTJ lies at the interface between MgO, the $1nm$ CoFeB layer, and the reference layer of MTJ lies at the interface between the $1.3nm$ CoFeB layer and the Co/Pt multilayer. The Landau-Lifshitz-Gilbert (LLG) equation governs these interfacial-free and reference layer magnetizations.

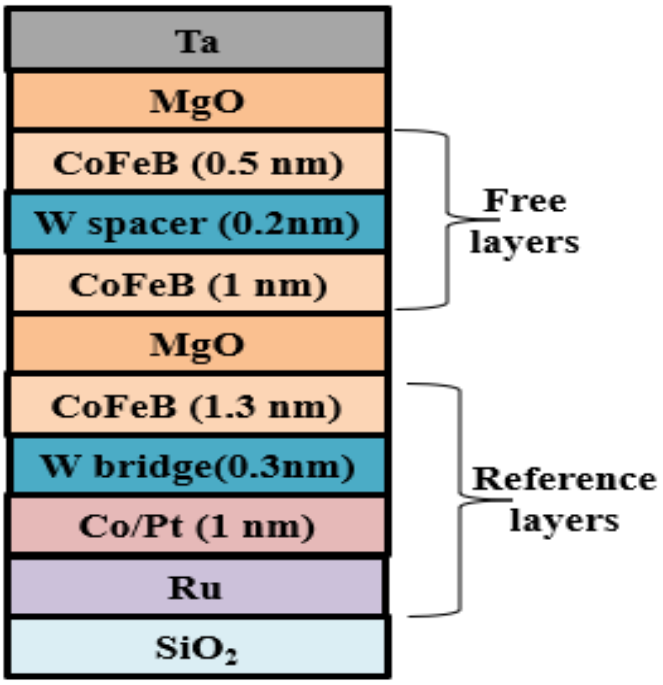


Figure 3: *Schematic of the p-MTJ stack structure with H.M./CoFeB/MgO composite.*

2.6. Micromagnetic simulation of toggled MRAM bit-cell

The toggled magnetic random-access memory (TST-MRAM) bit-cell can be designed by employing the VCMA effect. The charge precession of a nanoscale column structure is investigated and affected by spin-polarized currents and magnetic fields by MMS dependent on

the LLG condition, consolidating MRAM's toggle spin effects. It demonstrates the magnetic memory characterization by using ferromagnetic, nonmagnetic, and external field controls.

Fig. 4 demonstrates the MRAM bit cell has toggled memory operations, which are dependent on the spin-transfer-torque (STT) and spin-orbit-torque (SOT) mechanism [65-66]. The current pulses (I_{STT} and I_{SOT}) and magnetic field H are marked for the write operation. FL, PL, and TB denote the free layer. pinned layer, and tunnel barrier of MTJ. The heavy metal, source line, bit line, and write/read word line are indicated by $HM, SL, BL,$ and WWL/RWL.

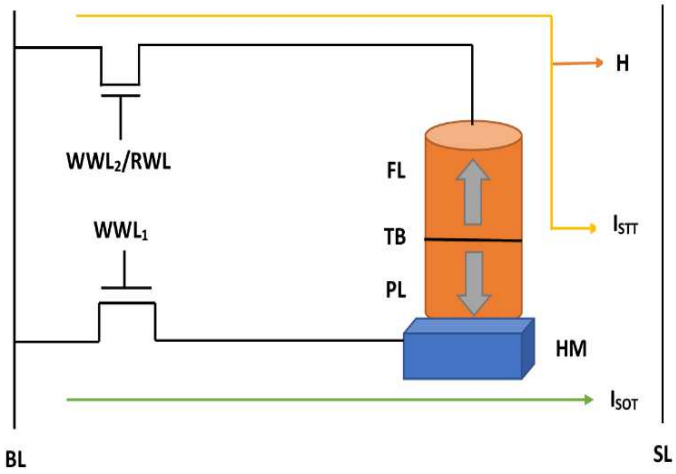


Figure 4: *Typical bit cell of the TST-MRAM memory unit. Schematic concept adapted from [33].*

This model's core concept is that the magnetic material's regulatory forces are sufficient to carry the magnetization in parallel over a characteristic length scale λ, just above the lattice constant a, denoted as:

$$S_i \approx S_j \; ; |x_i - x_j| < \lambda \gg a \; . \qquad (5)$$

where $S_{i/j}$ and $x_{i/j}$ are the distinct spins and their positions [65]. For a compatible density of spins, the discrete dissemination of magnetic moments S_i is approximated by a continuous vector density $M(x)$ such as [67]:

$$\int_{\Omega_0}^{\Omega_1} M(x)dx \approx \sum_i I_\Omega(x_i)S_i \; , \qquad (6)$$

It gives approximately true results for discretionary volumes Ω of the size $\lambda \times \lambda \times \lambda$ and greater, where I is the marker function [68]. It can be drafted in terms of a unit vector field, which is given below:

$$M(x) = M_s m(x) \; ; |m(x)| = 1 \qquad (7)$$

where M_s and $m(x)$ represent the saturation magnetization at $300k$ and the unit vector field of magnetization, respectively. The TST-MRAM bit cell considers micromagnetic modeling at $t = 0K$. The positive current is described as the current flowing from the free layer to the

pinned layer. The dynamics could be characterized by the transient advancement of the polarization M, and it complies with the summed-up Landau-Lifshitz-Gilbert-Slonczewski (LLGS) equation. Mathematically, this equation is represented as [68]:

$$\frac{d\vec{M}}{dt} = -\gamma\mu_0\left(\vec{M} \times \vec{H}_{eff}\right) + \frac{\alpha}{M_s}\left(\vec{M} \times \frac{\partial\vec{M}}{\partial t}\right) - \frac{\vec{M}\times(\vec{M}\times\vec{I}_s)}{qN_sM_s} \quad (8)$$

where γ is the electron's gyromagnetic ratio, $\vec{H}_{eff}$ is the effective magnetic field applied in nanomagnet, α is the dimensionless Gilbert damping constant, M_s is the nanomagnet's saturation magnetization, $\vec{I}_s$ is the applied spin current, q is the elementary charge, N_s is the number of spins, and V is the nanomagnet's volume.

An efficient field induces the spin-transfer torque, and this field is represented as:

$$H_{eff} = -\frac{1}{\mu_0}.\frac{\delta E}{\delta M}, \quad (9)$$

where H_{eff} is an effective field of the LLGS equation. It contains anisotropy, demagnetization, and external and exchange fields, which are represented as follows:

$$H_{eff} = H_{exch} + H_{ani} + H_{ms} + H_{ext}, \quad (10)$$

where H_{ms} is the demagnetization field.

The total energy E is expressed as:

$$E = E_{ani} + E_{exch} + E_{ms} + E_{ext}, \quad (11)$$

Here, E_{ani} is the anisotropy energy, E_{exch} is the exchange of energy, E_{ms} is the demagnetization energy, and E_{ext} is the external energy. The anisotropic energy of the CoFeB composite is represented as:

$$E_{ani} = \int (K_1[1 - m_s^2(r)] + K_2[1 - m_s^2(r)]^2)d^3r, \quad (12)$$

where K_1 and K_2 are the anisotropy constant, $m_s(r)$ is the entity magnetization vector at each grid at $K_1 > K_2$ under magnetization axis condition.

Exchange energy is represented as follows:

$$E_{exch} = \int \left(\frac{A}{M_S^2}|\nabla M(r)|^2\right) d^3r \quad (13)$$

where A is the exchange toughness constant.

3. RESULTS AND DISCUSSION

This section describes the development of interfaces between F.M.-N.M., N.M.-N.M., and H.M.-F.M.-N.M. using LLG equation-based parameters estimation for Stoiner physics particles. With the aid of MMS, the VCMA effect has been used to develop the TST-MRAM bit-cell. Table 1 displays the design specifications for the insignia made of ferromagnetic materials for the TST-MRAM cell, whereas Table 2 displays the insignia made of

paramagnetic materials for the TST-MRAM cell. For a given composite, it determines the magnetization factor, resistivity, AMR ratio, thickness of free space, and axis of current flow.

Table 1: *Characterization of ferromagnetic materials for the TST-VCMA model*

Parameters	**Valve**
Used Composite	CoFeB
Magnetization (KA/m)	950
Resistivity (μΩ-cm)	130
Relative Permeability	18000
Length of Free Space (nm)	70
Width of Free Space (nm)	70
Thickness of Free Space (nm)	1.49
Differ of X-axis Point from Origin (nm)	14
Differ of Y-axis Point from Origin (nm)	17
Differ of Z-axis Point from Origin (nm)	15
Azimuthal Angle for Initial Magnetic Orientation (degree)	71
Polar Angle for Initial Magnetic Orientation (degree)	60
Azimuthal Angle for Uniaxial Anisotropy (degree)	251
Polar Angle for Magnetic Uniaxial Anisotropy (degree)	210
Magnitude of Magnetic Uniaxial Anisotropy (KA/m)	150
Azimuthal Angle for Pinning Field (degree)	55
Polar Angle for Pinning Field (degree)	90
Magnitude for Pinning Field (KA/m)	25
AMR Ratio (%)	33.5 [66]
GMR Ratio (%)	56.4
Axis of Current Flow	X-axis

The Hamiltonian field is kept constant with an increase in Rashba SOI. The calculated value of the Hamiltonian field is $100\ KA/m^2$ due to the Rashba effect.

Table 2: *Characterization of paramagnetic materials for the TST-VCMA model*

Parameters	**Valve**
Used Composite	MgO
Magnetization (KA/m)	800
Resistivity (μΩ-cm)	75
Length of Free Space (nm)	70
Width of Free Space (nm)	70
Thickness of Free Space (nm)	1.4
Difference of X-axis Point from Origin (nm)	13
Difference of Y-axis Point from Origin (nm)	11
Differ of Z-axis Point from Origin (nm)	9
Azimuthal Angle for Initial Magnetic Orientation (degree)	9.87
Azimuthal Angle for Initial Magnetic Orientation (degree)	9.87
Polar Angle for Initial Magnetic Orientation (degree)	45
Azimuthal Angle for Magnetic Uniaxial Anisotropy (degree)	170.13
Polar Angle for Magnetic Uniaxial Anisotropy (degree)	156
Magnitude for Magnetic Uniaxial Anisotropy (KA/m)	110
Azimuthal Angle for Pinning Field (degree)	58.4
Polar Angle for Pinning Field (degree)	87.6
Magnitude for Pinning Field (KA/m)	25
AMR Ratio (%)	49.7 [67]
GMR Ratio (%)	23.5
Axis of Current Flow	Z-axis

Fig. 5 demonstrates the variation of conductance with the sensing voltage. The total conductance achieves a maximum value of 4.55 m℧ and a minimum value of 2.98 m℧ at $V_s = \pm 1.2$, and $0\ mV$.

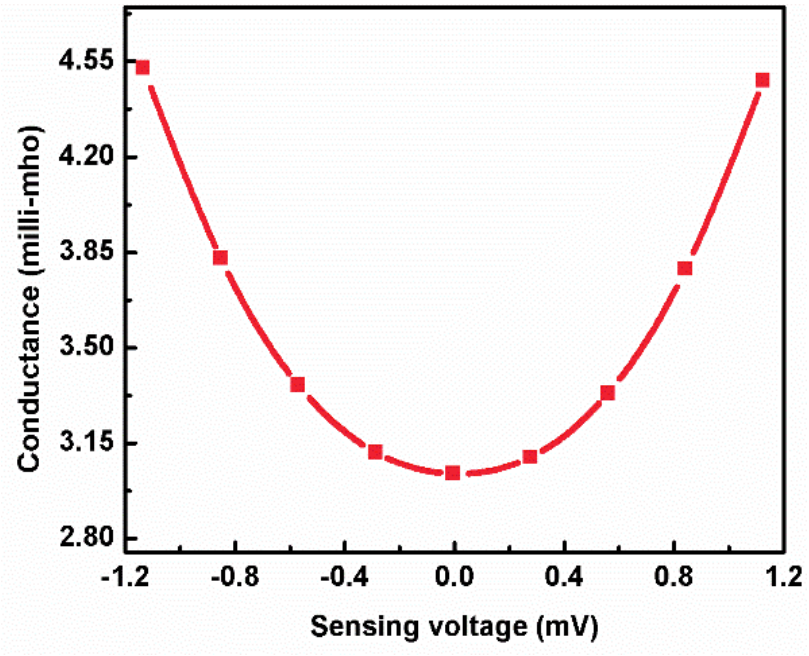


Figure 5: *Conductance representation of sensing voltage.*

The respective orientation of spin magnetization helped by ferromagnetic layers determines the conductivity of MTJ. The spins in both metallic layers must be parallel for MTJ to have the lowest conductivity. The highest conductivity of MTJ occurs when the spins are in opposition to each other. Fig. 6 represents the variation of the Hamiltonian field linearly with pinned layer thickness z. Hamiltonian field's maxima and minima have been achieved at $+300\ kA/m^2$ and $-300\ kA/m^2$, respectively. The thickness of the pinned layer controls the domain wall formation in CoFeB-dependent MTJs.

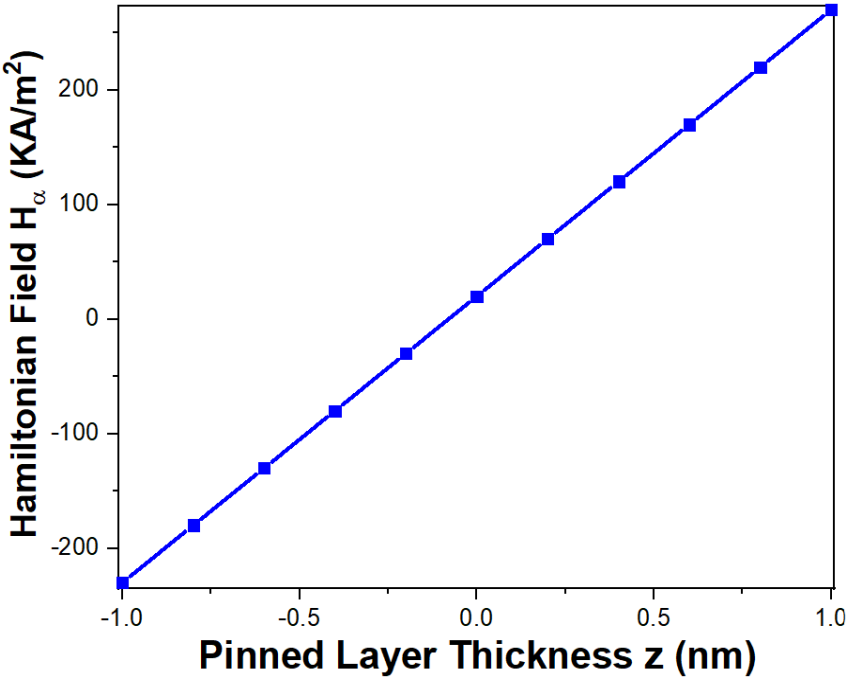


Figure 6: *Pinned field representation of the Hamiltonian field.*

Fig. 7 demonstrates that the magnetization in the x-direction varies exponentially with dynamic time t. The VCMA model computing parameter is magnetic polar orientation in a ferromagnetic layer by MMS. The maximum magnetization in the x-direction is $605\ kA/m$ at $t = 25ns$. The number of scans used in this process is 30.

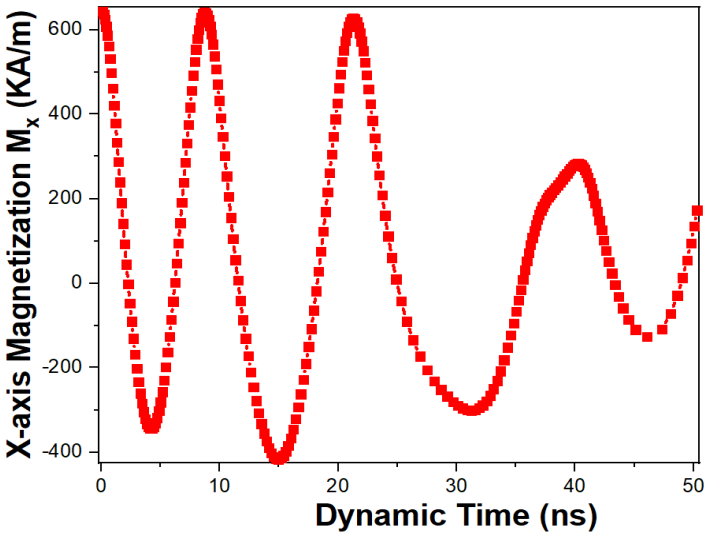


Figure 7: *Variation of magnetization in the x-direction with dynamic time t for calculating the magnetic polar orientation.*

Fig. 8 demonstrates the variation of magnetization in z-direction with dynamic time t. Due to the VCMA effect, the computing parameter is magnetic polar orientation in the ferromagnetic layer by micromagnetic modeling. The maximum magnetization in the z-direction is $320\ kA/m$ at $t = 37ns$. The maximum magnetic polar orientation is 70.995^0, according to the MMS result. It shows the highest magnetization in the z-direction and determines the damping profile of the proposed magnetic memory bit-cell.

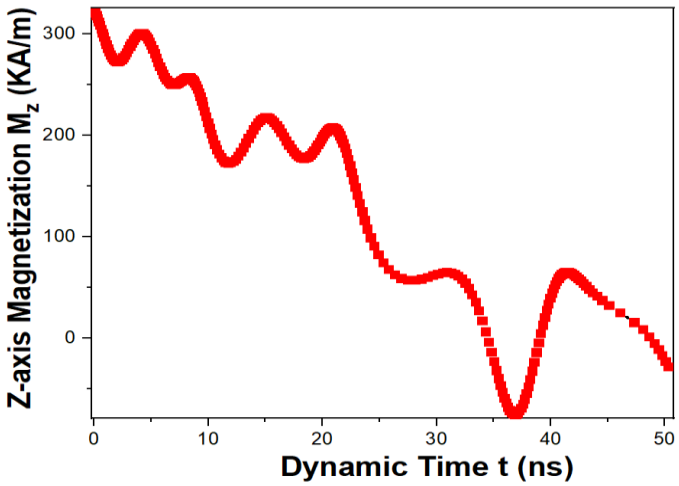


Figure 8: *Variation of magnetization in the z-direction with dynamic time t for calculating the magnetic polar orientation.*

Fig. 9 represents the variation of magnetization in the z-direction sinusoidally with dynamic time t. Because of the VCMA effect, the computing parameter is magnetic azimuthal orientation in the ferromagnetic layer by micromagnetic modeling. The maximum value (59.99^0) of magnetic azimuthal orientation is according to the MMS result. The maximum magnetization in the z-direction is $600\ kA/m$ at $t = 6ns, t = 18ns$, and $t = 40ns$.

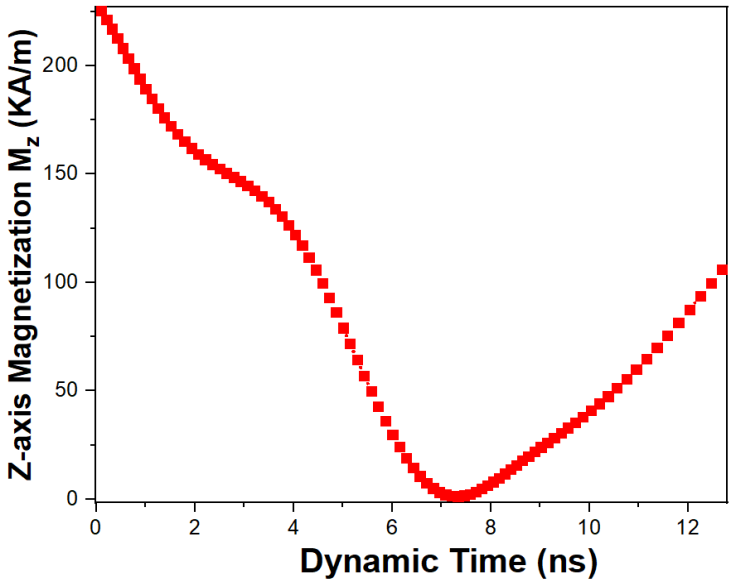


Figure 9: *Variation of magnetization in the z-direction with dynamic time t for calculating the magnetic azimuthal orientation.*

Fig. 10(a) demonstrates that the magnetization in the z-direction varies exponentially with dynamic time t, whereas Fig. 10(b) represents the physical layout of the toggled MRAM's ferromagnetic layer. The design of this layout has been created in response to the need for managing intensive magnetization switching and its spin-orbit coupling occurring at time intervals of $930\ ns$ and beyond. These actions are restricted to execution along the z-axis of switching to ensure both a notable speed of switching and a minimal error rate. The maximum magnetization factor has been successfully attained within the ferromagnetic layer of the toggled MRAM bit-cell. Principal magnetization in the ferromagnetic layer via micromagnetic modeling is the computing parameter owing to the VCMA effect. The MMS result indicates that the maximum principal magnetization is $950\,kA/m$. The maximum magnetization in the z-direction is $330\ kA/m$ at $t = 1ns$. The main goal of this device-level simulation is to configure the YZ-plane for the focal point switching mechanism and ensure that the magnetization is highest in the z-direction under all scenarios owing to this switching.

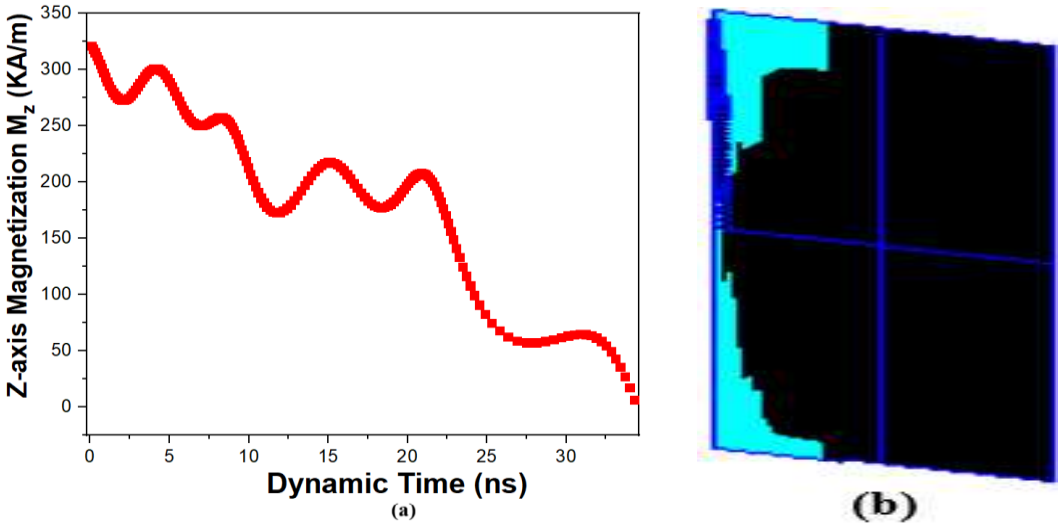


Figure 10: *(a) Variation of magnetization in the z-direction with dynamic time t for calculating the magnetization factor. (b) The physical layout of toggled MRAM's ferromagnetic layer.*

Fig. 11(a) depicts the exponential variation of magnetization in z-direction with dynamic time t, whereas Fig. 11(b) illustrates the physical layout of the toggled MRAM's ferromagnetic layer. The VCMA model's computing parameter is H_k azimuthal orientation in the ferromagnetic layer by micromagnetic modeling. The maximum H_k azimuthal orientation is 251^0, according to the MMS result. Therefore, the maximum magnetization in the z-direction is 180 kA/m at $t = 2ns$.

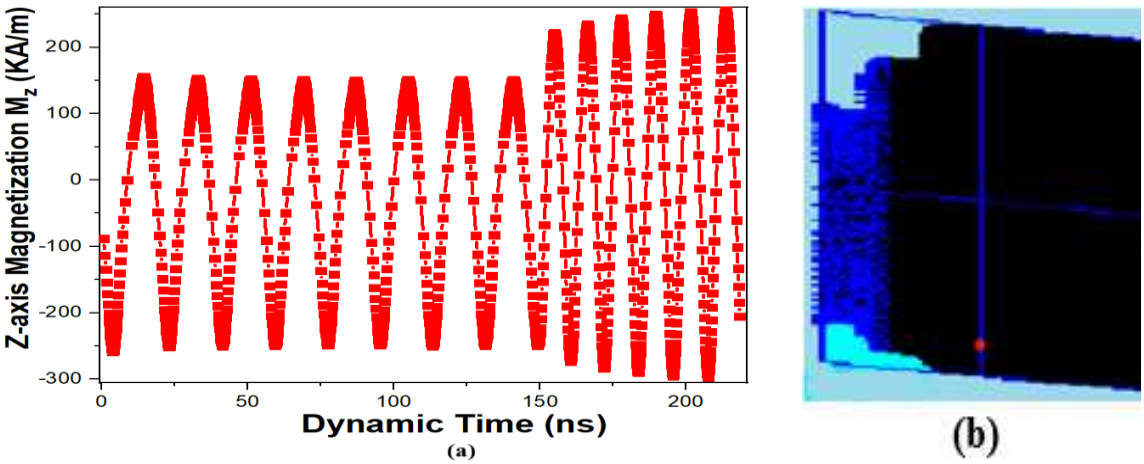


Figure 11: *(a) Variation of magnetization in the z-direction with dynamic time t for calculating the H_k azimuthal orientation; (b) The physical layout of toggled MRAM's ferromagnetic layer.*

Fig. 12 demonstrates that the magnetization in the y-direction varies exponentially with dynamic time t. Micromagnetic modeling of H_p polar orientation in the ferromagnetic layer serves as a computing parameter for the VCMA effect. By the MMS result, the maximum H_p polar orientation is 90^0. At t = 3 ns, it has a 610 kA/m maximum magnetization in the y-direction.

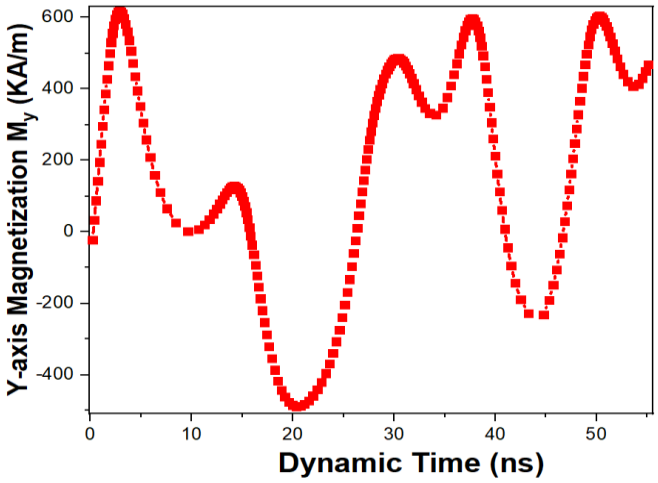


Figure 12: *Variation of magnetization in the y-direction with dynamic time t for calculating the H_p polar orientation.*

The toggled MRAM bit-cell design affected by the VCMA model is represented in Fig. 13. The axis ratio is 34:56 for MMS. The total used dynamic time is $2.03\mu s$ for toggle-based magnetic memory cell development.

Dynamic Calculation:

Total Time (0.01 ns) = 2027.207, Scale (X: Z) = 34:56

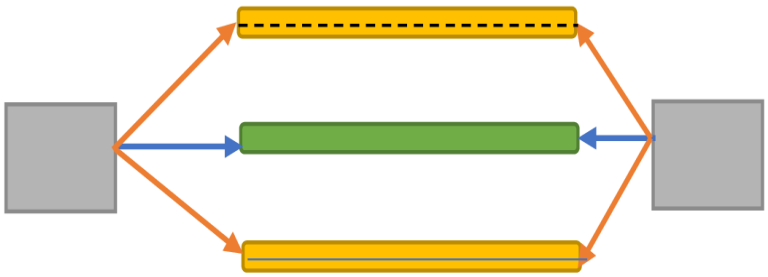


Figure 13: *Toggled MRAM ferromagnetic bit-cell design assisted by VCMA effect.*

Fig. 14 represents the variation of net magnetization exponentially with dynamic time t. The computing parameter is the principal magnetization in the ferromagnetic layer by micromagnetic modeling and is 220 kA/m at $t = 25ns$ because of the VCMA effect. The maximum principal magnetization is 800 kA/m, according to the MMS result. It is possible to determine the forces that emerge from these interactions using magnetization, which specifies how a material reacts to an applied magnetic field in addition to how it modifies the magnetic field. Three-dimensional visualization of the net magnetization is feasible. The number of scans used in this process is 10.

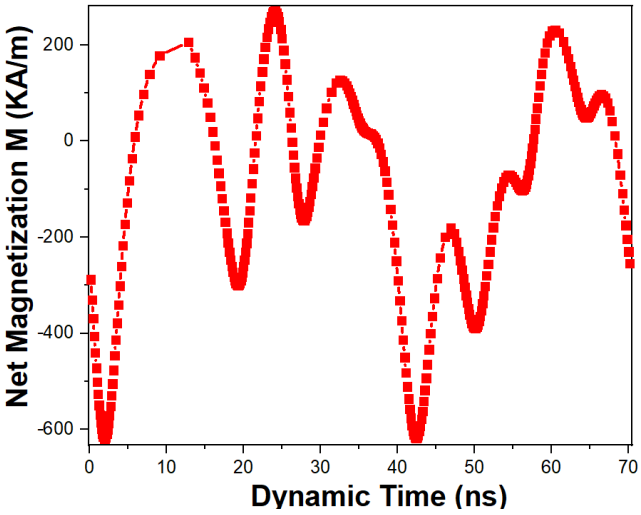


Figure 14: *Variation of net magnetization with dynamic time t for calculating the magnetization factor.*

Fig. 15(a) demonstrates that the net magnetization varies exponentially with dynamic time t, whereas Fig. 15(b) represents the physical layout of toggled MRAM's nonmagnetic layer. The design of this layout has been created in response to the need for managing net magnetization switching and its spin-orbit interaction occurring at time intervals of 870 ns and beyond. The execution of these actions is limited to the z-axis of switching to guarantee both a noteworthy switching speed and a streamlined design. The shortest channel length has been effectively achieved within the nonmagnetic layer of the toggled MRAM bit-cell. Due to the VCMA effect, the computing parameter is channel length in the nonmagnetic layer by micromagnetic modeling. The maximum channel length is $70nm$, according to the MMS result. Hence, the maximum net magnetization is 615 kA/m at $t = 19ns$.

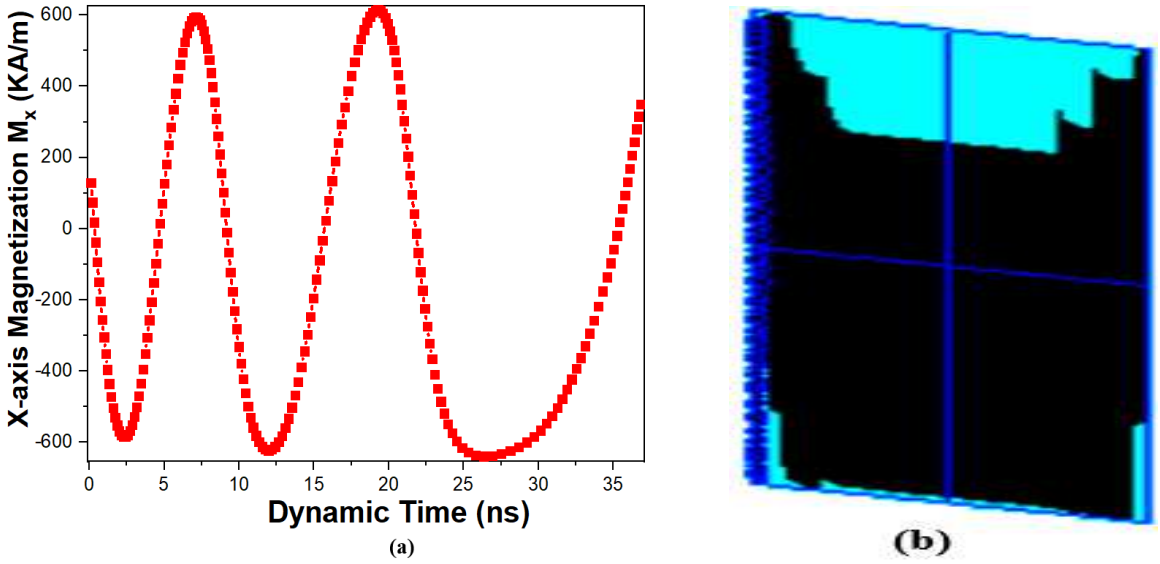


Figure 15: *(a) Variation of net magnetization with dynamic time t for calculating the channel length; (b) The physical layout of toggled MRAM's nonmagnetic layer.*

The toggled MRAM bit-cell design affected by the VCMA model is represented in Fig. 16. The axis ratio is 32:49 for MMS by Simulmag software. The total used dynamic time is 2.02 μs for toggle-based magnetic cell development.

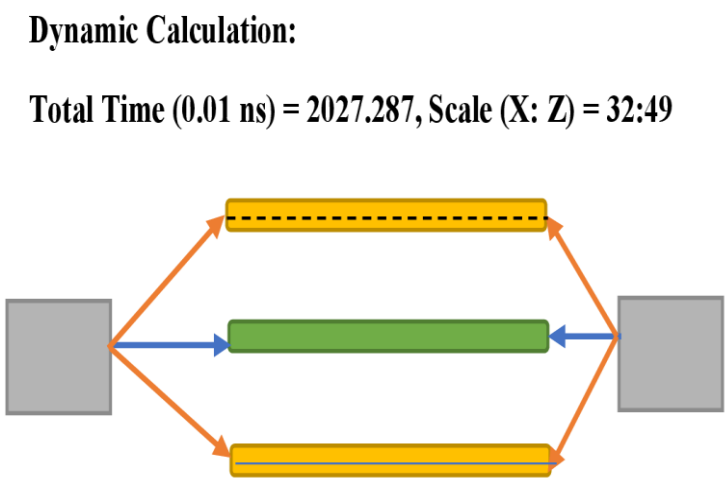


Figure 16: *Toggled MRAM nonmagnetic bit-cell design assisted by VCMA effect.*

Fig. 17(a) depicts the sinusoidal variation of magnetization in the x-direction with dynamic time t, whereas Fig. 17(b) illustrates the physical layout of a toggled MRAM controlled by an external field. Because of the VCMA effect, the computing parameter is the pulse-field amplitude in the external field controlled by micromagnetic modeling. The maximum pulse-field amplitude is 114 kA/m as per the MMS result. The total number of scans used in this process is 15. The maximum magnetization in the y-direction is 620 kA/m at $t = 11ns, t = 31ns$, and $t = 51ns$.

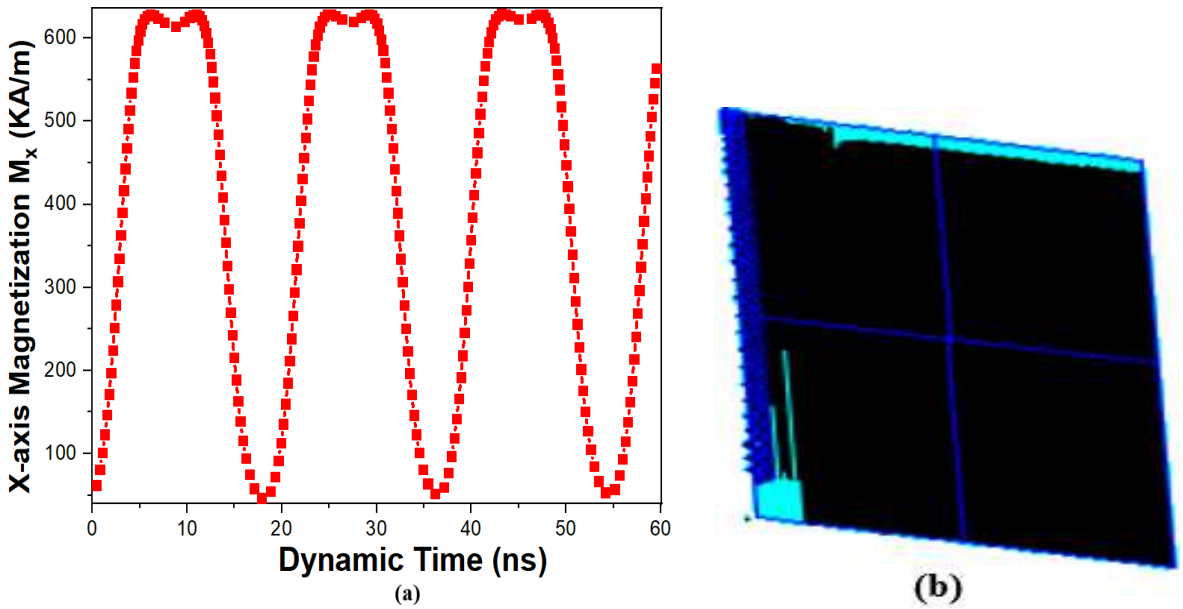


Figure 17: *(a) Variation of magnetization in the x-direction with dynamic time t for calculating the pulse field amplitude; (b) The physical layout of toggled MRAM's external field layer.*

Fig. 18 represents the comparison curve between magnetization variations in the y-direction exponentially with dynamic time t. The pulse-field rise time denotes the period of a memory module that shows the power requirement of a current pulse in the intermediate state. The maximum pulse-field rise time and pulse-field azimuth angle are $3.85ns$ and 71^0 as per the MMS results. Therefore, the maximum magnetization in the y-direction is $640\ kA/m$ at $t = 39ns$. The pulse-field azimuth angle describes the angular dimension of a current pulse in a spherical coordinate system and can be determined with the help of a magnetic compass. The intersection point is achieved at $46\ ns$ in the process of evaluating the pulse field rise time and azimuth angle.

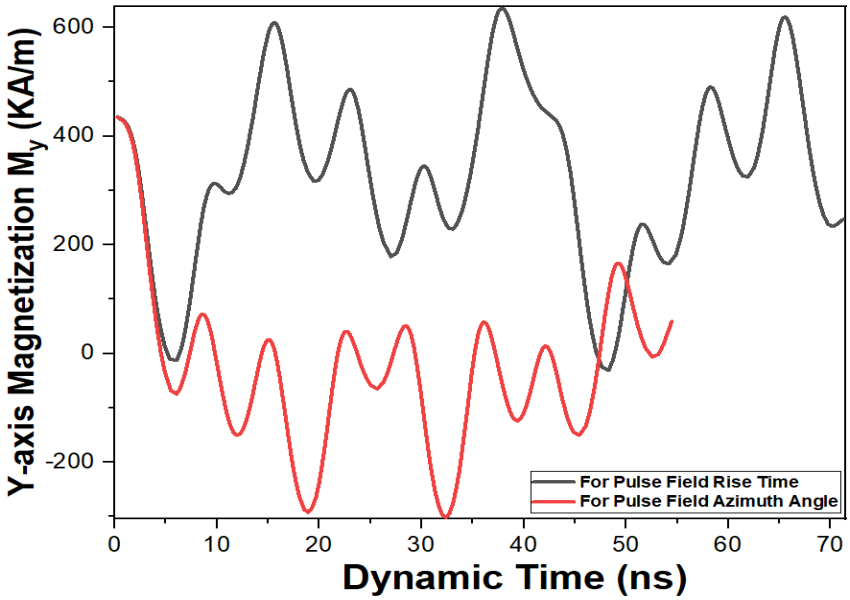


Figure 18: *Comparison between magnetization variation in the y-direction with dynamic time t for calculating the pulse field rise time and pulse field azimuth angle.*

Table 3: *Parameters of designed TST-MRAM's bit cell*

Parameters	**Valve**
Channel length (nm)	70
Magnetic polar orientation (degree)	70.9
Magnetic anisotropy field (kA/m)	1884.9
Magnetic azimuthal orientation (degree)	59.9
Resistivity $(\mu\Omega - cm)$	130
Relative X origin (nm)	14
Relative Y origin (nm)	17

Pinning field (kA/m)	314.1
Relative permeability	18000
Damping constant $(GHz - m/kA)$	0.0035
H_p polar orientation (degree)	90
H_k polar orientation (degree)	210

The calculated values of the designed MRAM bit cell's parameters are tabulated in Table 3. The toggled MRAM bit-cell design affected by the VCMA model is represented in Fig. 19. The axis ratio is 32:49 for MMS. The total dynamic time is $2.04\,\mu s$ for toggle-based magnetic memory cell development. Figs. 13, 16, and 19 describe the characterization differences and impact of ferromagnetic, nonmagnetic materials, and external fields on a toggled MRAM bit-cell.

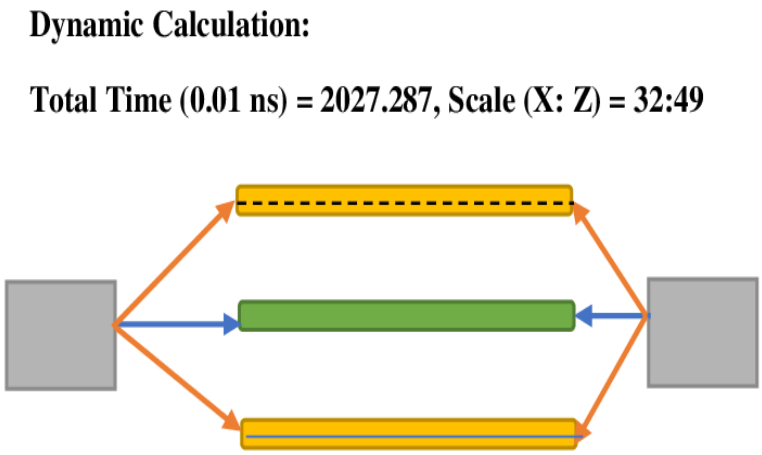


Figure 19: *VCMA-assisted toggled MRAM bit-cell design controlled by an external field.*

The application of the VCMA effect has led to notable improvements in the read and write access times of the toggled MRAM bit-cell, showcasing enhancements of 216% and 568% compared to the STT-MRAM cell, as well as improvements of 113% and 366% compared to the SOT-MRAM cell [68]. The optimization of the magnetization factor in the toggled memory bit-cell has resulted in gains of 22% and 17% when compared to the STT-MRAM and SOT-MRAM cells, respectively. Furthermore, the damping ratio has experienced a significant increase of 403% and 416% in contrast to the in-plane MTJ (IMTJ) and interfacial perpendicular MTJ (iPMTJ) configurations [69-70] of the STT-MRAM cell. Conversely, the polarization factor has been reduced by 22% and 26% compared to the STT-MRAM and SOT-MRAM cells, respectively. Notably, the anisotropic coefficient is found to be 21 times

greater than that of the STT-MRAM cell and 20 times greater than that of the SOT-MRAM cell.

4. CONCLUSION

Spintronics has been explored for ultra-low power and sub-nanoseconds switching regime MRAM devices. This work presents the design of the toggled MRAM bit-cell with the help of an MMS-based approach. The advantages of the proposed design are a lower damping ratio, higher anisotropic coefficient, fast switching, and low switching power requirements. The VCMA effect is utilized to achieve the efficient performance of the designed bit-cell. The damping ratio, magnetization factor, and polar and azimuthal orientation are the essential parameters to create an efficient toggled MRAM bit-cell. The simulated results verify the device modeling and develop memory layout in two-dimensional spaces. As a result, the designed bit-cell achieves better performance as compared to other state-of-the-art designs. The toggled MRAM bit-cell can be utilized in the fields of aerospace, memory storage, quantum computing, and space applications. Although not discussed here, another direction toward achieving high-performance memory cells in spin-based computers is the deployment of domain wall logic. The future generation of computing units will be heavily empowered by the upcoming generations of spin-based memory and its applications.

Declaration of competing interest

The authors declare that they have no known competing financial interests or personal relationships that could have influenced the work reported in this paper.

Data Availability Statement

No data is associated with this manuscript.

Declaration of Funding: The authors declare that there is no funding received for this work.

REFERENCES

[1] J. Fabian, Spintronics Physics, *Condens. Matter Phys.* 34, 434441 (2009).

[2] J. Fabian, A. Matos-Abiague, C. Ertler, P. Stano, I. Zutic, Semiconductor Spintronics, *Acta Phys. Slovak.* 57, 565907 (2007).

[3] I. Adagideli, G.E.W. Bauer, Detection of current-induced Spins by Ferromagnetic Contacts, *Phys. Rev. Lett.* 97, 256601 (2006).

[4] S. Bhatti, R. Sbiaa, A. Hirohata, H. Ohno, S. Fukami, Spintronics based random access memory: A review, *Mater. Today* 20, 530548 (2017).

[5] J. I. Raffel, T. S. Crowther, A proposal for an associative memory using magnetic films, IEEE Trans. Electro. Comput. 13, 611615 (1964).

[6] M. N. Baibich, J.M. Broto, A. Fert, F.N.V. Dau, F. Petroff, Giant magnetoresistance of (001) Fe/ (001) Cr magnetic superlattices, *Phys. Rev. Lett.* 21, 2472475 (1988).

[7] G. Binasch, P. Grünberg, F. Saurenbach, W. Zinn, Enhanced magnetoresistance in layered magnetic structures with the antiferromagnetic interlayer exchange, *Phys. Rev. B* 39, 4828 (1989).

[8] T. Miyazaki, N. Tezuka, Giant magnetic tunneling effect in Fe/Al2O3/Fe junction, *J. Magnet. Magn. Mater.* 139, L231 (1995).

[9] J. S. Moodera, L. R. Kinder, T. M. Wong, and R. Meservey, Large magnetoresistance at room temperature in ferromagnetic thin film tunnel junctions, *Phys. Rev. Lett.* 74, 3273276 (1995).

[10] J.C. Slonczewski, Current-driven excitation of magnetic multilayers, *J. Magnet. Magn. Mater.* 159, L1-L7 (1996).

[11] L. Berger, Emission of spin waves by a magnetic multilayer traversed by a current, *Phys. Rev. B 54*, 9353 (1996).

[12] J. A. Katine, F. J. Albert, R. A. Buhrman, D. C. Ralph, Current-driven magnetization reversal and spin-wave excitations in Co/Cu/Co pillars, *Phys. Rev. Lett.* 14, 3149 (2000).

[13] W. Kim, J. H. Jeong, Y. Kim, W. C. Lim, J. H. Kim, Extended scalability of perpendicular STT-MRAM towards sub-20 nm MTJ node, *Inter. Elect. Dev. Meeting*, 531534 (2011).

[14] M. Gajek, J. J. Nowak, J. Z. Sun, P. L. Trouilloud, Spin Torque Switching of 20 nm magnetic tunnel junction with Perpendicular anisotropy, *Appl. Phys. Lett.* 13, 132408 (2012).

[15] T. Kawahara, K. Ito, R. Takemura, and H. Ohno, Spin-transfer torque RAM Technology: Review and prospect, *Microelect. Reliability* 52, 2012.

[16] A. V. Khvalkovskiy, D. Apalkov, S. Watts, Basic Principles of STT -MRAM cell operation in memory arrays, *Appl. Phys. Lett.* 46, 2013.

[17] Q. J. Yap, J. J. Qiu, P. Luo, J. F. Ying, G. C. Han, D. E. Laughlin, J. G. Zhu, T. Kanbe, T. Shige, Phase ordering and its effect on the magnetic and structural property of FeRh ultrathin films, *J. Appl. Phys.* 4, 043902 (2014).

[18] B. N. Engel, J. Akerman, B. Butcher, R. W. Dave, S. Tehrani, A 4-Mb toggle MRAM based on a novel bit and switching method, *IEEE Trans. Magnet.* 41, 1 (2005).

[19] Saied Tehrani, Status and Outlook of MRAM Memory Technology, *Inter. Electro. Dev. Meeting* (USA, 2006).

[20] J. M. Slaughter, N. D. Rizzo, J. Janesky, R. Whig, F. B. Mancoff, D. Houssameddine, J. J. Sun, S. Aggarwal, K. Nagel, S. Deshpande, S. M. Alam, T. Andre, and P. LoPresti, High-density ST-MRAM technology, *Inter. Electro. Dev. Meeting* (USA, 2012).

[21] S. Yuasa, A. Fukushima, K. Yakushiji, T. Nozaki, M. Konoto, H. Maehara, H. Kubota, T. Taniguchi, H. Arai, H. Imamura, K. Ando, Y. Shiota, F. Bonell, Y. Suzuki, N. Shimomura, E. Kitagawa, J. Ito, S. Fujita, K. Abe, H. Noguchi, and H. Yoda, Future prospects of MRAM technologies*, IEEE Inter. Electro. Dev. Meeting* (USA, 2013).

[22] M. Durlam, D. Addie, J. Akerman, B. Butcher, A 0.18μm 4Mb Toggling MRAM, *IEEE Inter. Electro. Dev. Meeting*, 2004.

[23] T. Min, Z. Tokei, G. Sankar Kar, S. Coseman, Interconnects scaling challenge for sub-20nm spin torque transfer magnetic random-access memory technology, *IEEE Inter. Interconn. Technol. Conf.* (USA, 2014).

[24] T. Min, Q. Chen, R. Beach, G. Jan, A study of write margin of spin torque transfer magnetic random-access memory technology, *IEEE Trans. Magnet.* 46, 2010.

[25] P. Khalili, K. Wang, Electric-field-controlled MRAM based on voltage control of magnetic anisotropy (VCMA): Recent progress and perspectives, *4th Berkeley Sympos. Energy Efficient Electro. Syst.*, (USA, 2015).

[26] P. Amiri, K. Wang, K Galatsis, Voltage-controlled magnetic anisotropy (VCMA) switch and magneto-electric memory (MeRAM), *U.S. Patents*, US9324403B2 (2015).

[27] C. Grezes, F. Ebrahimi, J. G. Alzate, X. Cai, J. A. Katine, J. Langer, K.L. Wang, Ultra-low switching energy and scaling in electric-field-controlled nanoscale magnetic tunnel junctions with the high resistance-area product, *Appl. Phys. Lett.* 108, 2016.

[28] A. D. Karenowska, A. V. Chumak, A. A. Serga, and B. Hillebrands, Magnon Spintronics, *Nature Phys.* 11, 453 (2015).

[29] Haiming Yu, Jiang Xiao, Helmut Schultheiss, Magnetic texture based magnonics, *Phys. Reports* 905, 1 (2021).

[30] T. Jungwirth, X. Marti, P. Wadley, J. Wunderlich, Antiferromagnetic Spintronics, *Nature Nanotechnol. J.* 11, 231241 (2016).

[31] W. Granig, C. Kolle, D. Hammerschmidt, B. Schaffer, R. Borgschulze, C. Reidl, J. Zimmer, Integrated gigant magnetic resistance-based angle sensor, *IEEE Sensors Conference* (South Korea, 2007).
[32] C. Abert, Micromagnetics and Spintronics: models and numerical methods, *Euro. Phys. J.* 92, 2019.
[33] D. Jain, and S. Dahiya, Modeling for Improved Performance of Ultra-Fast Non-volatile Toggle Spin Torque MRAM Bit-Cell, SPIN 12, 2250013 (2022).
[34[R. Hao, L. Wang, and T. Min, A Novel STT-MRAM design with electric-field-assisted synthetic antiferromagnetic free layer, *IEEE Transac. Magnet.* 55, 2019.
[35] C. Yoshida, T. Tanaka, T. Ataka, A. Furuya, Micromagnetic Study of Probabilistic Switching Behavior in Sub 200nm CoFeB/MgO Magnetic Tunnel Junction, *Non-Volatile Memory Technol. Sympos.* (NVMTS), 2018.
[36] H. B. Huang, X. Q. Ma, Z. H. Liu, X. M. Shi, T. Yue, Z. H. Xiao, and L. Q. Chen, Micromagnetic simulation of spin transfer torque magnetization precession phase diagram in a spin-valve nanopillar under external magnetic fields, *ISRN Condens. Matter Phys.* 12, 387380 (2012).
[37] P. F. Carcia, A. D. Meinhaldt, A. Suna, Perpendicular magnetic anisotropy in Pd/Co thin film layered structures, *Appl. Phys. Lett.* 47, 178 (1985).
[38] J. Wang, Y. Bai, H. Wang, Z. Hao, G. Wang, K. Zhang, Y. Zhang, W. Lu, Y. Zhang, Reconfigurable Bit-Serial Operation Using Toggle SOT-MRAM for High-Performance Computing in Memory Architecture, IEEE Transac. Circ. Sys. I, 2022.
[39] Y. Zhang, J. Wang, C. Lian, Y. Bai, G. Wang, Z. Zhang, Z. Zheng, L. Chen, Time-Domain Computing in Memory Using Spintronics for Energy-Efficient Convolutional Neural Network, IEEE Trans. Circ. Syst. I-68, 11931205 (2021).
[40] P. F. Carcia, Perpendicular magnetic anisotropy in Pd/Co and Pt/Co thin film layered structures, *Appl. Phys. Lett.* 63, 5066 (1988).
[41] S. Hashimoto, Y. Ochiai, K. Aso, Perpendicular magnetic anisotropy and magnetostriction of sputtered Co/Pd and Co/Pt multi-layered films, *J. Appl. Phys.* 66, 4909 (1989).
[42] J. H. Park, C. Park, T. Jeong, M. T. Moneck, N. T. Nufer, Co/Pt multilayer based magnetic tunnel junctions using perpendicular magnetic anisotropy, *J. Appl. Phys.* 103, 07A917 (2008).
[43] D. Lim, K. Kim, S. Kim, W. Y. Jeung, Study on exchange-biased perpendicular magnetic tunnel junction based on Pd/Co multilayers, *IEEE Transact. Magnet.* 6, 2009.
[44] R. Law, R. Sbiaa, T. Liew, T. C. Chong, Magnetoresistance and switching properties of Co-Fe/Pd-based perpendicular anisotropy single- and dual-spin valves", *IEEE Trans. Magnet.* 44, 11 (2008).
[45] M. Gottwald, J. J. Kan, K. Lee, X. Zhu, C. Park, Scalable and thermally robust perpendicular magnetic tunnel junctions for STT-MRAM, *Appl. Phys. Lett.* 106, 032413 (2015).
[46] K. Yakushiji, A. Sugihara, A. Fukushima, H. Kubota, S. Yuasa, Very strong antiferromagnetic interlayer exchange coupling with iridium spacer layer for perpendicular magnetic tunnel junctions, *Appl. Phys. Lett.* 110, 092406 (2017).
[47] S. Andrieu, T. Hauet, M. Gottwald, P. Ohresser, Co/Ni multilayers for spintronics: High spin polarization and tunable magnetic anisotropy, *Phys. Rev. Mater.* 2, 064410 (2018).
[48] J. M. L. Beaujour, W. Chen, C. C. Kao, Ferromagnetic resonance study of sputtered Co/Ni multilayers, *Euro. Phys. J.* 59, 475483 (2007).
[49] G. H. O. Daalderop, P. J. Kelly, Prediction and conformation of perpendicular magnetic anisotropy in Co/Ni multilayers, *Phys. Rev. Lett.* 68, 682 (1992).
[50] M. Gottwald, S. Andrieu, F. Gimbert, L. Calmels, Co/Ni (111) superlattices studied by microscopy, X-ray absorption, and ab initio calculations, *Phys. Rev. B* 86, 014425 (2012).
[51] G. S. Kar, W. Kim, T. Tahmasebi, J. Swerts, S. Mertens, T. Min, Co/Ni-based p-MTJ stack for sub-20nm high density stand-alone and high-performance embedded memory application, *IEEE Inter. Elect. Dev. Meeting*, 2014.
[52] P. K. Amiri, Z. M. Zeng, J. Langer, H. Zhao, G. Rowlands, Y.-J. Chen, I. N. Krivorotov, J.-P. Wang, H. W. Jiang, J. A. Katine, Y. Huai, K. Galatsis, K. L. Wang, Switching current reduction using perpendicular anisotropy in CoFeB-MgO magnetic tunnel junctions, *Appl. Phys. Lett.* 98, 112507 (2011).

[53] H. Meng, R Sbiaa, C. C. Wang, S. Y. H. Lua, Annealing temperature window for tunneling magnetoresistance and spin torque switching in CoFeB/MgO/CoFeB perpendicular magnetic tunnel junctions, *J. Appl. Phys.* 110, 103915 (2011).

[54] S. Ikeda, K. Miura, H. Yamamoto, M. Endo, A perpendicular anisotropy CoFeB-MgO magnetic tunnel junction, *Nature Mater. 9*, 721724 (2010).

[55] M. T. Johnson, P. J. H. Bloemen, J. J. de Vries, Magnetic anisotropy in metallic multilayers, *IOP Scien. Rep. Prog. Phys.* 59, 1996.

[56] H. X. Yang, M. Chshiev, J. H. Lee, A. Manchon, First-principles investigation of the very large perpendicular magnetic anisotropy at Fe|MgO and Co|MgO interfaces, *Phys. Rev. B* 84, 054401 (2011).

[57] A. Hallal, H. X. Yang, B. Dieny, Anatomy of perpendicular magnetic anisotropy in Fe/MgO magnetic tunnel junctions: First-principles insight, *Phys. Rev. B* 88, 184423 (2013).

[58] S. Nazir, S. Jiang, J. Cheng, K. Yang, Enhanced interfacial perpendicular magnetic anisotropy in Fe/MgO heterostructure via interfacial engineering, *Appl. Phys. Lett*. 114, 072407 (2019).

[59] N. Roschewsky, S. Schafer, F. Hellman, V. Nikitin, Perpendicular magnetic tunnel junction performance under mechanical strain, *Appl. Phys. Lett.* 112, 232401 (2018).

[60] M. Cubukcu, O. Boulle, J. Langer, G. Gaudin, Spin-orbit torque magnetization switching of a three-terminal perpendicular magnetic tunnel junction, *Appl. Phys. Lett.* 104, 042406 (2014).

[61] K. Mizunuma, S. Ikeda, H. Ohno, K. Miura, Tunnel magnetoresistance properties and annealing stability in perpendicular anisotropy MgO-based magnetic tunnel junctions with different stack structures, *J. Appl. Phys.* 109, 07C711 (2011).

[62] W. X. Wang, Y. Yang, H. Naganuma, X. F. Han, Y. Ando, The perpendicular anisotropy of $Co_{40}Fe_{40}B_{20}$ sandwiched between Ta and MgO layers and its application in CoFeB/MgO/CoFeB tunnel junction, *Appl. Phys. Lett.* 99, 012502 (2011).

[63] N. Miyakawa, D. C. Worledge, K. Kita, Impact of Ta diffusion on the perpendicular magnetic anisotropy of Ta/CoFeB/MgO, IEEE Magnet. Lett. 4, 2013.

[64] Z. Wang, H. Zhou, M. Wang, W. Cai, D. Zhu, W. Zhao, Proposal of Toggle Spin Torques Magnetic RAM for Ultrafast Computing, *IEEE Elec. Dev. Lett.* 4, 726729 (2019).

[65] T. Schre, G. Hrkac, S. Bance, D. Suess, O. Ertl, J. Fidler, Numerical methods in micromagnetics (finite element method), *Handbook Magnet. Advan. Magnet. Mater.*, 2007.

[66] Y. Huai, Spin-transfer torque MRAM (STT-MRAM): challenges and prospects, *IEEE Dev. Resear. Conf.* 18, 2009.

[67] S.S. Parkin, C. Kaiser, A. Panchula, P.M. Rice, B. Hughes, M. Samant, S.-H. Yang, Giant tunneling magnetoresistance at room temperature with MgO (100) tunnel barriers, *Nature Mater.* 3, 862867 (2004).

[68] T. Nozaki, A. K. Rachwał, W. Skowroński, V. Zayets, Y. Shiota, S. Tamaru, H. Kubota, A. Fukushima, and S. Y. Y. Suzuki, Large voltage-induced changes in the perpendicular magnetic anisotropy of a MgO-based tunnel junction with an ultrathin Fe layer, *Phys. Rev. Appl.* 5, 044006 (2016).

[69] T. L. Gilbert, A phenomenological theory of damping in ferromagnetic materials, *IEEE Transac. Magnet.* 40, 3443 (2004).

[70] W. H. Butler, T. Mewas, P. B. Visscher, S. E. Russek, Switching distributions for perpendicular spin-torque devices within the macrospin approximation*, IEEE Trans. Magnet.* 48, 4684 (2012).